Journal of Structural Geology 31 (2009) 654–661

Contents lists available at ScienceDirect

Journal of Structural Geology

journal homepage: www.elsevier.com/locate/jsg

Interpreting finite strain: Analysis of deformation in analog models

Saad S.B. Haq [a,*], Dan M. Davis [b]

[a] Department of Earth and Atmospheric Sciences, Purdue University, 550 Stadium Mall Drive, Civil Eng. Building, West Lafayette, IN 47906, USA
[b] Department of Geosciences, Stony Brook University, Stony Brook, NY 11790, USA

ARTICLE INFO

Article history:
Received 28 October 2008
Received in revised form
5 March 2009
Accepted 10 March 2009
Available online 15 April 2009

Keywords:
Strain
Deformation analysis
Analog model
Strain partitioning
Sandbox experiments

ABSTRACT

We investigate the accuracy of strain rates calculated directly from a robust set of velocity measurements that were obtained in controlled experimental settings. We compare the calculated strains and strain rates, and the corresponding deformation style, determined from sets of three vs. four velocity measurements obtained by tracking a dense set of surface markers during experiments. The density of our measurements, in conjunction with a well-understood model deformational setting, allows us to relate the style and magnitude of strains to the underlying structures. We demonstrate that calculating *strain values* from three measurements can be irrelevant to the geologic structures even if they are mathematically correct, but that one can avoid some of these deceptive results by using quadrangles to calculate strain. We demonstrate the utility of such strain calculations in interpreting strain partitioning in obliquely convergent analog models for continuously and discontinuously deforming materials. In addition, we compare direct calculations with those obtained by determining strains from the derivatives of continuous spline functions that have been fit to the velocity field.

1. Introduction

Measurements of local crustal velocity fields are frequently used to understand observed deformation in the context of larger-scale plate motions. Likewise, precise measurement of displacements in analog models and calculation of the corresponding strain fields can contribute greatly to the effectiveness of such models for testing ideas about the mechanics of such plate boundary regions. Our goal is to compare sandbox deformation with nature to understand better the tectonics of orogenic belts, particularly for oblique convergence or complex plate geometries. The key geologic observables, such as rock deformation and seismic moment, that reveal past and ongoing deformation are, of course, governed by strain rather than displacement or velocity. It is therefore essential to extract from displacement measurements in analog models the best possible values for the distribution of strain and strain rate across the model orogens.

Strain is reference frame independent, depending only upon displacement gradients. However, a single set of observed displacements can yield very different solutions for the strain field depending upon how the observations are grouped. In an attempt to quantify the style and magnitude of deformation in analog models we have precisely measured the surface displacements resulting from convergence in analog models. To achieve our overall goal of comparing sandbox deformation with natural orogens we must obtain strain estimates that are indicative of the actual structural development that is occurring within the experiment.

In the controlled and well-characterized 'tectonic' setting of an analog model we can examine the accuracy of strain fields calculated solely from velocity measurements. This allows us to test the validity of a range of assumptions that may be made when using a 2D-velocity field to quantify strain rates, both in nature and in analog and numerical modeling.

Analog modeling has successfully improved our understanding of convergent margin mechanics, providing insight into the development of broadly useful analytical models (e.g., Hubbert and Rubey, 1959; Davis et al., 1983; Koons and Henderson, 1995; Wang and Davis, 1996; Mulugeta, 1988; Martinez et al., 2002; McClay et al., 2004; Haq and Davis, 2008). The usefulness of analog models stems from the inherent 3-dimensionality of the deformation and the relative simplicity with which experimental parameters, such as boundary conditions and geometry, can be tested.

In the experiments described here, we used a large motor-driven 'sandbox' apparatus in which deformation is monitored with a digital camera for the duration of the experiment. Applying techniques often used in remote sensing and geodesy (e.g., Jensen, 2000), we track the displacement of surface markers to determine finite deformation. In each experiment, we make a large number of direct measurements of displacement, from which we calculate velocity, strain, and strain rate fields, and monitor the growth of

* Corresponding author. Tel.: +1 765 496 7206.
E-mail address: shaq@purdue.edu (S.S.B. Haq).

0191-8141/$ – see front matter © 2009 Elsevier Ltd. All rights reserved.
doi:10.1016/j.jsg.2009.03.017

topography. These measurements provide comparison to numerical techniques or geophysical data, such as earthquake mechanisms and GPS velocities (Haq, 2004).

2. Examples of strain calculation

The determination of a physically representative, as opposed to mathematically accurate but geologically uninformative, value of strain (or strain rate) requires careful design of the network for sampling the displacement (or velocity) field. As we demonstrate below, this becomes particularly important when, as is now possible in analog modeling, the distribution of measurements approaches the same length scale as the deformation. The example in Fig. 1 is also used to give a geologic context for the calculations and the analog models in this paper.

To calculate deformation each network can be sampled by either triangles or as quadrilaterals. Four stations arranged in a quadrilateral (Fig. 2) can be arranged in either of two possible triangle-pair combinations: in this case, upper-left and lower-right (UL–LR Fig. 2A) and lower-left and upper-right (LL–UR Fig. 2B), as well as the quadrilateral itself (Fig. 2C). The five 'X' marks in these figures represent the centroids (polygon center-of-area points) where we plot the calculated strain values – the four values from the triangles and the quadrilateral ('Quad') strain calculated from their area-weighted average. In the following examples, the principal strain axes are calculated for the three possible networks corresponding to each region: two triangle-based networks and one based on quadrilaterals. Determining 2-D strain directly from displacement gradients requires only three observations. However, as we will demonstrate, such a calculation can easily lead to a solution that is not physically meaningful. For this reason, we have developed an algorithm that utilizes pairs of side-sharing triangles to determine the area-weighted strain of the corresponding quadrilateral.

The four points of a quadrilateral at which velocities are determined define four triangles. Using the finite strain equations of Means (1976), we determine the strain (strain rate) tensor for each triangle. The triangles may be grouped in two ways to calculate velocity gradients and to encompass the entire quadrilateral ('A' vs. 'B' in Fig. 2). For each possible triangle pairings, we determine a strain tensor by an area-weighted average of the corresponding tensor components corresponding to the paired triangles. Each of the two pairings may give a slightly different solution for the strain, and it is not always possible to know *a priori* which triangle pairing will yield a more accurate and physically meaningful result. Therefore, we use the average of the strain tensor components from both sets of triangle pairings to determine the quadrangle strain (or strain rate) tensor. While this algorithm sacrifices some of the resolution available with triangle-based calculations, it consistently determines a more meaningful solution for strain in our analog models. Polygons are particularly useful for determining finite strain in analog models as marker points are inevitably lost and the grid becomes very irregular (Appendix Fig. 1).

We use the treatment of Means (1976) for determining the Lagrangian 2-d finite strain tensor (E_{ij}), where

$$E_{ij} = \frac{1}{2}\left[\frac{\partial u_i}{\partial X_j} + \frac{\partial u_j}{\partial X_i} + \frac{\partial u_k}{\partial X_i}\frac{\partial u_k}{\partial X_j}\right] \tag{1}$$

and u_i and u_j are the displacements and X_i and X_j are the lengths in the Cartesian directions.

Below are two of the four terms that arise from the expansion of the tensor notation in Equation (1).

$$E_{11} = \frac{1}{2}\left[\frac{\partial u_1}{\partial X_1} + \frac{\partial u_1}{\partial X_1}\right] + \frac{1}{2}\left[\frac{\partial u_1}{\partial X_1}\frac{\partial u_1}{\partial X_1} + \frac{\partial u_2}{\partial X_1}\frac{\partial u_2}{\partial X_1}\right] \tag{2}$$

and

$$E_{12} = \frac{1}{2}\left[\frac{\partial u_1}{\partial X_2} + \frac{\partial u_2}{\partial X_1}\right] + \frac{1}{2}\left[\frac{\partial u_1}{\partial X_1}\frac{\partial u_1}{\partial X_2} + \frac{\partial u_2}{\partial X_1}\frac{\partial u_2}{\partial X_2}\right] \tag{3}$$

note that as the displacements become smaller, the higher-order terms in Equations (2) and (3) quickly become insignificant and these finite strain equations reduce to the expressions for instantaneous strain. Therefore finite strain equations are valid to use for small displacements.

The principal axes directions and magnitudes, determined from the finite strain tensors, are plotted as red (contraction) and blue (extension) vectors (Figs. 3 and 4). In each of the two triangle pairs (UL–LR and LL–UR), strain tensor values are averaged to provide an accurate value for mean strain across the entire quadrangle. Their average is plotted as the 'Quadrangle' strain and is the first solution in each row of Figs. 3 and 4 (See tables in Appendix for the positions, velocities, and calculated strain tensors illustrated by these figures).

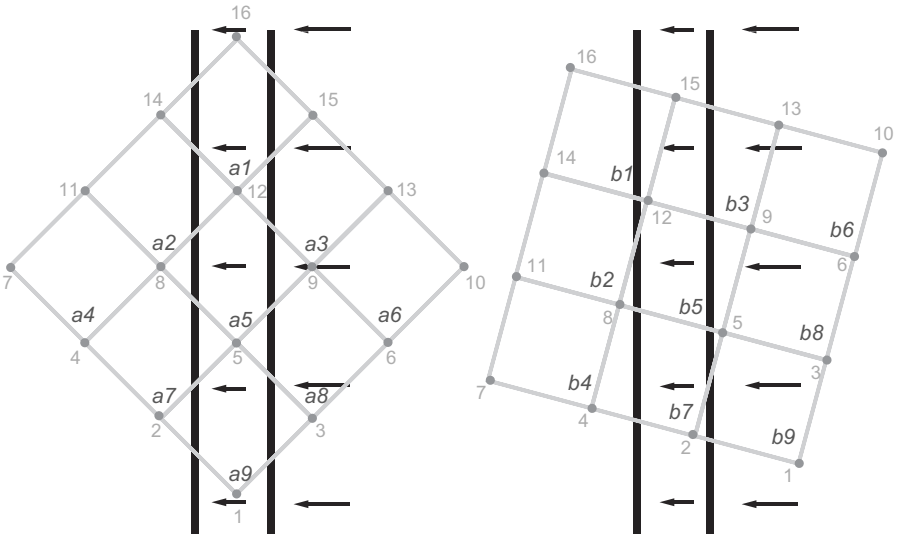

Fig. 1. A and B: Thrust faults sampled by two different displacement-measurement networks. A pair of thrust faults (vertical black lines) that are encompassed within two 16-station (numbered in grey) networks. In each configuration, the faults slip the same amount but are arranged differently within the respective sub-networks (four stations).

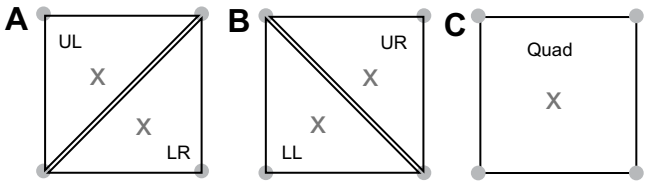

Fig. 2. A–C: Possible connections from a simple four-station network. The 'X' marks the spot where the principal strains will be plotted for the corresponding triangle or quadrangle.

The calculation of the strain in any particular part of the simple examples in Fig. 1 or in our analog models begins with the grouping of the sets of 'stations' (analog experiment marker dots) that correspond to velocity measurements for calculating strain. In particular, the use of triangles (3 measurements) or quadrangles (four measurements from pairs of side-sharing triangles) needs to be evaluated. Whether the deformation occurred on discrete faults or in a viscous, distributed manner, it may be homogeneous on the scale of the sampling network (left side of Fig. 3). Likewise (right side of Fig. 3) it may be inhomogeneous on the scale of the network elements. In the latter case, the strain calculated using individual triangles is dependent upon the orientation of each triangle with respect to the deformation field – a problem that is alleviated by using a quadrilateral composed of a pair of those same triangles (Fig. 2C). Fig. 1A represents the case in which deformation, either homogeneous or inhomogeneous, is fortuitously distributed evenly and symmetrically across much of the network within the quadrangles. In general, however, this optimal orientation with respect to the deformation is not achieved for the individual triangles.

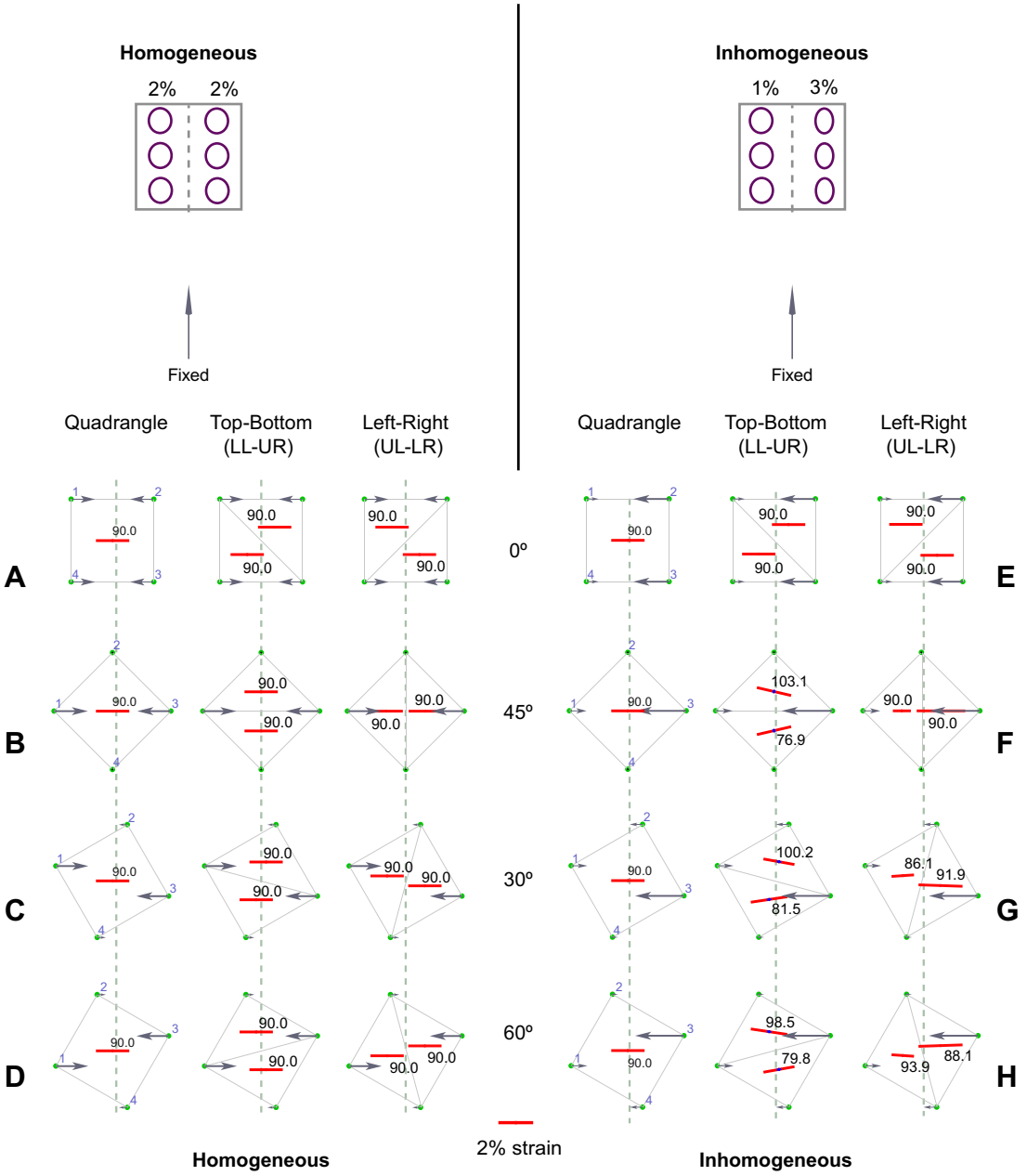

Fig. 3. Simple set of calculations of strain for a strain field that is homogeneous (A–D) or inhomogeneous (E–H) over the length scale of a single set of four displacement-measurement points. The grey arrows indicate the displacements used in each calculation. In each network the same bulk deformation is sampled. These displacement fields can result from either discrete or continuous deformation. Note that while triangle-pair solutions vary greatly the quadrangles are consistent.

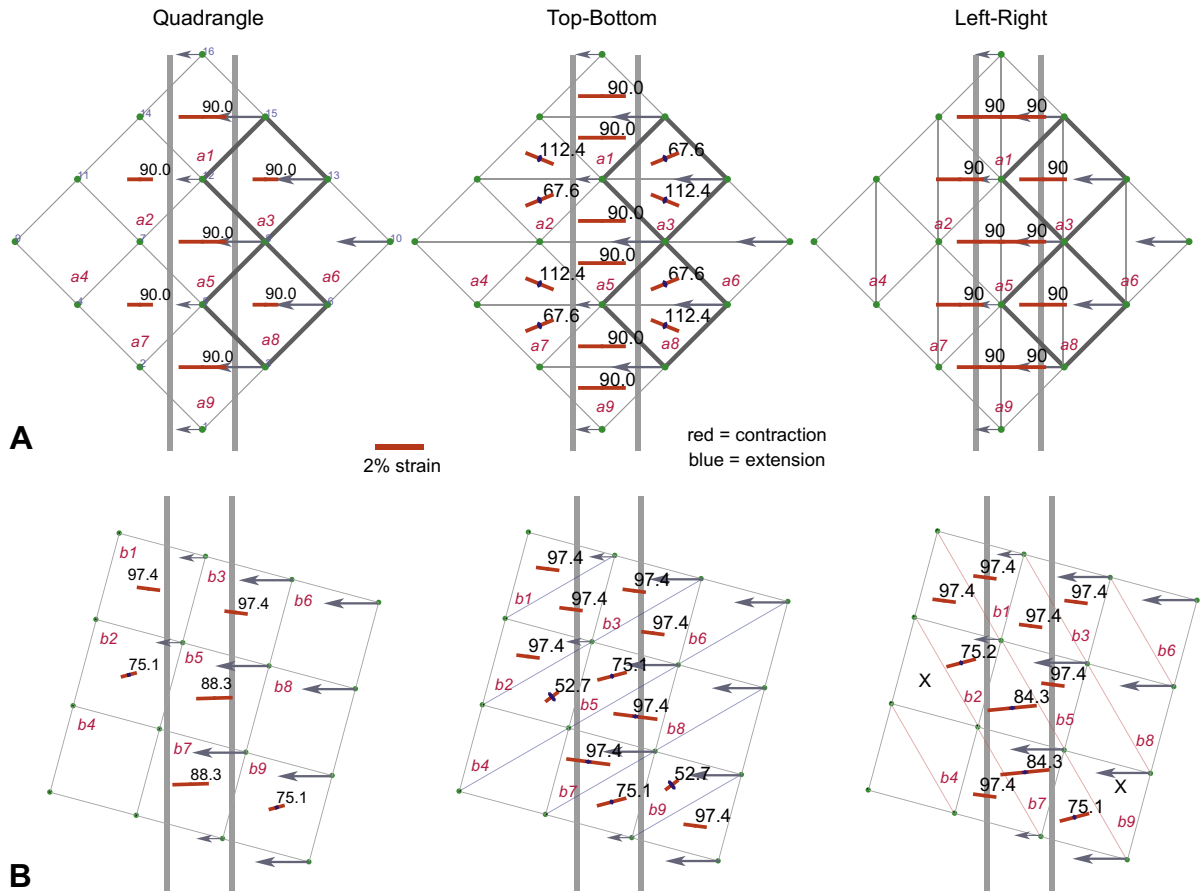

Fig. 4. Strain calculated for a pair of thrust faults using two different networks. The principal strain axes are indicated by red (contraction) and blue (extension) lines that are scaled by strain magnitude. In each case, the azimuth of the most contractional principal strain is indicated in black above the strain axes. In configuration 4A, the structures are symmetrically sampled in the quadrangles, each of which therefore gives a consistent solution for the strain field. In Fig. 4B, the network is rotated by 30°, and the component triangles of each quadrangle do not symmetrically sample the faults, so the quadrangles also yield variable solutions for the strain. The values in black are the azimuths of the principal contraction axes.

When the points for velocity measurement are widely spaced with respect to discrete faulting (or the faulting is closely and evenly spaced within the network), the deformation field is indistinguishable from a smooth field, not unlike an evenly stretched rubber sheet. In that case (Fig. 3 A–D), the strain values derived from triangles are independent of point sampling – the calculated strain is always correct and geologically meaningful with respect to the net displacement due to faulting.

If, however, the deformation is unevenly distributed within the sub-networks (Fig. 3 E–H), calculated strain using groupings of three points does not represent the deformation style except for a fortuitous geometry. In contrast, the corresponding quadrangle often yields calculated strains indicative of deformation style even when triangles do not (Fig. 3 F–H).

Although it is not standard procedure to use triangles in natural zones of deformation, it may be tempting to do so in the data-rich environment of analog modeling. However, a random grid geometry or inhomogeneity of strain greatly limits the utility of this approach (Figs. 3F–H and 4B) even in a continuous medium. Consider, for example, the highlighted polygons a3 and a8 across Fig. 4A. As illustrated in Fig. 1, we know that the region is undergoing east–west contraction by two dip-slip faults. Each triangle in polygons a3 and a8 (Fig. 4A) samples at most one fault. The left–right triangle-pair solution samples the deformation ideally, showing east–west shortening on the left and no deformation on the right. The top and bottom triangles, however, each have two points on the same (rightmost) thrust sheet and one on the middle sheet, between the two faults. That point moves with respect to the other two in a direction that is oblique to the line between them, in a clockwise sense for the top triangle and a counter-clockwise sense for the bottom one – introducing an inevitable handedness to the calculated velocity gradients and strains. This effect is clearest with discrete faults but can also occur with continuous deformation when strain gradients occur.

The left–right triangle pair in Fig. 4A gives the correct answer with better spatial resolution than a polygon, whereas the top–bottom triangles give physically meaningless strain values with regard to the faulting despite being mathematically accurate. In this case the polygon average value invariably gives a geologically and mathematically correct answer. This last result is not surprising, as the same total strain exists within the region.

The strains calculated for the triangles and polygon for the rotated network in Fig. 4B, however, are all very different. The calculated strains do not represent the true 'tectonics' of east–west contraction, as calculated for Fig. 1 and Fig. 4A. While the average polygon value for the top–bottom triangles in the optimally oriented network in Fig. 4A gives the expected answer, none of the solutions for the triangle pairings in Fig. 4B are indicative of the actual sense of east–west contraction. In Fig. 1B or Fig. 4B, it is important to note that the deceptiveness of such strain calculations is not an artifact of the particular network geometry, nor of the relative orientation of the fault slip. The non-physical result of

Fig. 4B is the rule for discrete faulting, where the sample network for displacement measurement has a spacing comparable to that of the individual structures accommodating deformation. This situation is the case except for a limited number of network orientations with special triangle symmetry, such as the example in Figs. 1A and 4A, and of a grid rotated 45° from it. Because networks in analog models can be very dense compared to the scale of the structures, the spacing and orientation of those networks is consequently a particularly important consideration for tracking strain in analog models.

In these examples, with their simply defined tectonic style, an asymmetry in deformation clearly does not exist physically but appears in some calculations of strain, particularly when measurements are taken on a scale that is comparable to or smaller than the individual structures, such that multiple points of a single strain-calculation quadrangle are located on the same thrust sheet. Such difficulties are to be expected as the measurement network becomes similar in spacing to the scale of the discrete structure. The recognition of such misleading results, which is obvious in this idealized setting and in the simplest analog models, may be far more problematical when dealing with measurements in more complex experiments for which, like the Earth, the actual deformation is not well known. Even when the deformation is regionally homogenous (e.g., continuous deformation or evenly spaced faults with equal slip), as network scale approaches that of the structures, the sampling of the active structures can yield a solution for strain that lacks physical insight, precluding comparison of analog model results to natural orogens.

This result is further demonstrated in an analog modeling experiments of convergent settings, described below, where motion is oblique to the model margin, and strain is being actively partitioned. Analog modeling permits an arbitrarily large number of strain marker points so the density and location of points is typically not a constraint in obtaining high spatial resolution on strain measurements. On the other hand, if a strain-calculation triangle or quadrilateral is located entirely within a single thrust sheet in a highly deforming region, it will yield essentially zero strain. Conversely, depending on the sampling, highly localized strain from faulting can be smeared out over large regions. Even with an initial network spacing that is dense compared to the developing structures, this can be a consideration in analog modeling if marker dots have disappeared by having been overthrust (or lost due to extension).

3. Overview of the modeling technique

Our experimental procedure has two distinct aspects: analog modeling, which is similar in its implementation to our earlier models (e.g., Haq and Davis, 1997, 2008), and the automated acquisition of XY-coordinate data that are used to determine net velocity and the deformation tensor. The basic configuration consists of an analog forearc, including a 'backstop' (e.g., Byrne et al., 1993; Haq and Davis, 2008), which is configured here as a Plexiglas plate in front of a pushing backwall (Fig. 5B). Once the experimental geometry is configured, a uniformly thick layer of material to simulate sedimentary rocks of the upper crust is placed over the plates (Fig. 5B). We have characterized the yield properties for these frictional and viscous materials, which deform as a result of displacement of the plate by the backwall. The frictional material is a weakly dilatant, subangular carbonate sand with a density of 1.65 g cm^{-3}, a static internal friction coefficient of approximately 0.56 (internal friction angle $\varphi = 29°$), and time-independent frictional behavior at reasonable displacement strain rates (Byerlee, 1978; Paterson, 1978). The ductile material is a viscous gel with a density of 1.32 g cm^{-3} and a nearly Newtonian viscosity of approximately 10^5 Pa over a wide range of strain rates. Below about 10 Pa, it displays Bingham behavior and ceases to flow. During an experiment, a sequence of digital images of the model surface (in plan-view) is obtained from a fixed position relative to the pushing backwall, at small intervals, using a digital camera (Haq, 2004).

An initially rectangular grid of marker points or 'geodetic stations' on the surface of the sand is tracked for the purpose of determining a continuous displacement field for the duration of the experiment. The velocities determined for a given image pair are networked together in order to determine a strain rate field. Any subset of at least three connected points in the network is sufficient to determine an XY-plane strain rate tensor as well as the no-length-change directions, and (if desired) the dilatation, shear strain and rotation rate fields. With this technique, the locations of the 'stations' are determined to a very high precision (the darkness-weighted midpoints of the dots are reproducible to better than 0.1 mm). With the acquisition of numerous high-resolution images, quantitative examination of the development of structures during the experiment is achievable with sufficient spatial and temporal resolution. By employing an automated algorithm, we correlate the locations of marker points in subsequent images and determine the polygon networks. We then can easily and accurately calculate the surface velocity (displacement rate) and strain rate fields over numerous intervals. In each interval, we apply a Lagrangian approach to calculating strain (Means, 1976), using only those marker points that have survived without being over-thrust and for which we can determine coordinates with a high confidence. With this technique we add rigorous deformation analysis to our analog modeling, which has already proven to be a robust modeling tool for examining deformation.

To determine a dense velocity field from which to obtain a highly resolved deformation field, we employ a network of marker points containing roughly 1400 points in a 2.5 cm spacing, about half of which become visible to the camera only when brought into the field of view after additional convergence. Although our grid starts out as regularly spaced, large finite strains during the experiment quickly lead to an irregularly spaced network (See Appendix, Fig. A1) that is constantly tracked and regridded when necessary throughout the experiment. As the eventual location and orientation of the model structures with respect to the grid is not initially known, the initial network configuration can affect the usefulness of the solution in interpreting deformation in an experiment.

4. Discrete deformation (frictional models and faulting)

Thus far, the discussion has been supported by calculations for hypothetical deformation. In the next few examples, we show how grid geometry and polygon choice can influence or obscure the analysis of strain in analog models. In Fig. 6A–D, we use an analog model to illustrate how sampling biases strain determination even where the deformation is simple and well known. Fig. 6 shows an early stage of an analog model of a convergent margin with a 45° obliquity to plate motion, in which the strain patterns are relatively simple and predictable. Using the displacement field in Fig. 6A we calculate the strain for the three possible network geometries described in Fig. 2, the top–bottom (UL–LR), and left–right (LL–UR) triangle pairs and the quadrangle average. In evaluating the effect of the network on strain determination the choice of network geometry can greatly affect the style of the resulting strain field, and thus its interpretation, even with numerous and precise velocity measurements. For example, in Fig. 6B the network does not optimally sample the active accommodating structures. The style of calculated strain, with adjacent triangles alternating

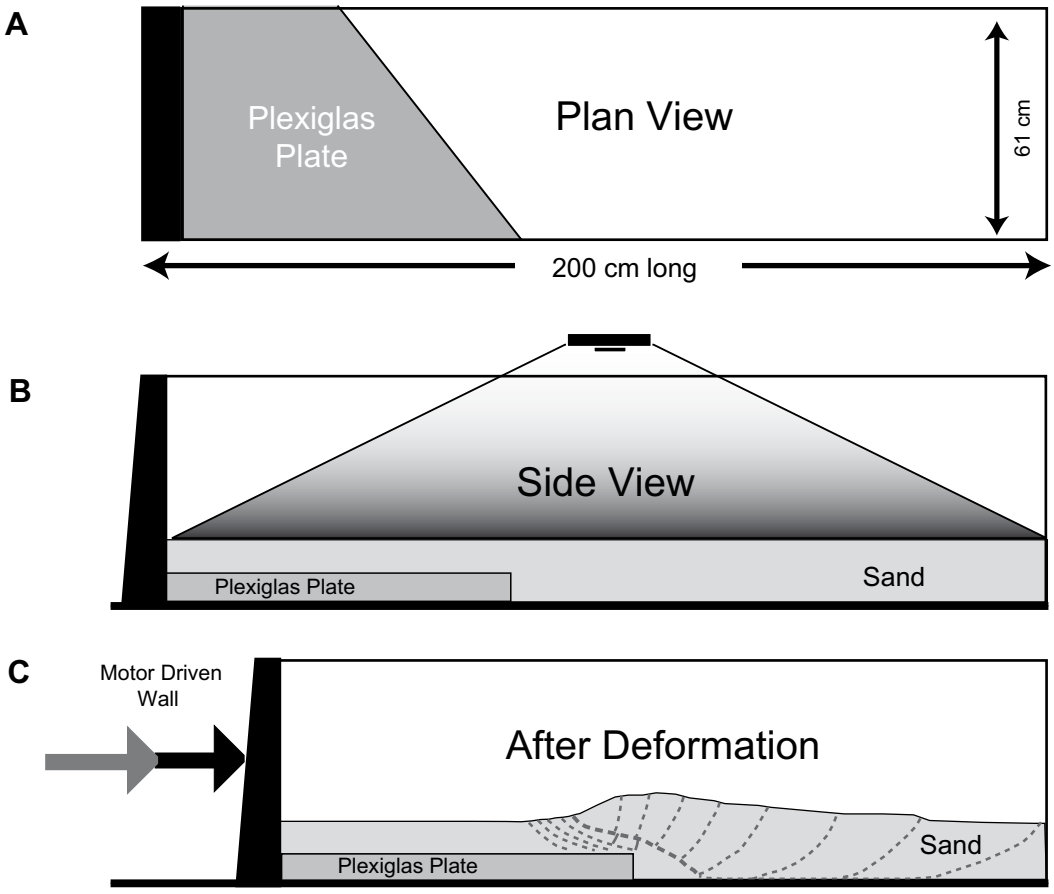

Fig. 5. Sandbox Schematic. A) Plan-view schematic of the lab apparatus. A motor-driven moving wall pushes a block corresponding to the over-thrusting plate, causing translation and deformation in front of it. A digital camera rides over the box, moving with the wall. B) Side-view schematic. Note the deforming material (in this case, a contractional wedge made of sand) lying on top of the base of the box (the lower plate) and the rigid basement block of the upper plate. The location of the digital camera is directly above the deforming region. C) Side-view schematic after convergent deformation. Dashed lines indicate discrete thrust faults.

between along-strike extension and strike-slip shear, does not reflect the actual deformation that is occurring.

The along-strike variability in the calculated strain can generate a regular but alternating pattern that may be mathematically correct based on the displacements but does not correctly represent the deformation of the thrust fault system. Even when deforming structures generally intersect the network at ideal orientations for sampling, as in the very early stages of this experiment, not every triangle will give a solution that is physically meaningful. Note the column (black arrow) of largely extensional principal axes, Fig. 6C. This extension is spurious and not reflecting reality as no dip-slip extension occurs in the model. Just to the left of that column of strain axes there is a transition to strike-slip deformation style, indicated by roughly equal lengths of blue extension to red contraction axes, which is more accurate for that portion of the model.

As suggested earlier, in a dense network the simplest solution to this potential ambiguity would be to take the average value of pairs of triangles, which are often more representative of the actual deformation. The improved solution, using quadrangles, is plotted in Fig. 6D where the triangle-pair averages are calculated from those in Fig. 6B and C. By using quads, we trade some spatial resolution for a solution that is more robust in areas across the deforming region. While the systematic artifact in Fig. 6B or C is obvious, in experiments with less regular geometries, the problem may be less easy to detect. Therefore, we believe that it is preferable to use quadrangles rather that triangles when possible, despite the resultant loss of resolution.

5. Continuous deformation (viscous model – no faults)

In the examples to this point, the velocity calculations reflected shortening accommodated by discrete frictional faulting. The precise value of strain, however, is undefined (a singularity) at these points. In practical applications, the locations of all the structures accommodating displacement are frequently not known in advance. For this reason, we also present an experiment where deformation is continuous in a viscous medium, for an initial geometry and subsequent model plate displacement history that is similar to that for the deformation of the sand body. By sampling with triangles and quadrangles in both frictional and viscous experiments, we show that the ambiguity in deformation style does not depend upon the singularities such as discrete faults in the deformation field but is instead, only a function of sampling procedure (Fig. 7). Thus, for distributed (as well as discrete) deformation, non-optimal strain-calculation triangles may greatly misrepresent the actual deformation style.

Theoretical predictions (e.g., Platt, 1993; Enlow and Koons, 1998), as well as observations of strain indicators and earthquake focal mechanisms in natural convergence (e.g., Jarrard, 1986; McCaffrey, 1996), suggest that shortening axes around the deformation front for oblique convergence should be intermediate between the plate convergence direction and the normal to strike. In examining Figs. 6D and 7D, we see that analog models behave in precisely this manner, partitioning part of the margin-parallel component of convergence into strain within the orogen (Haq and Davis, 2005). This observation, true for both frictional (Fig. 6) and

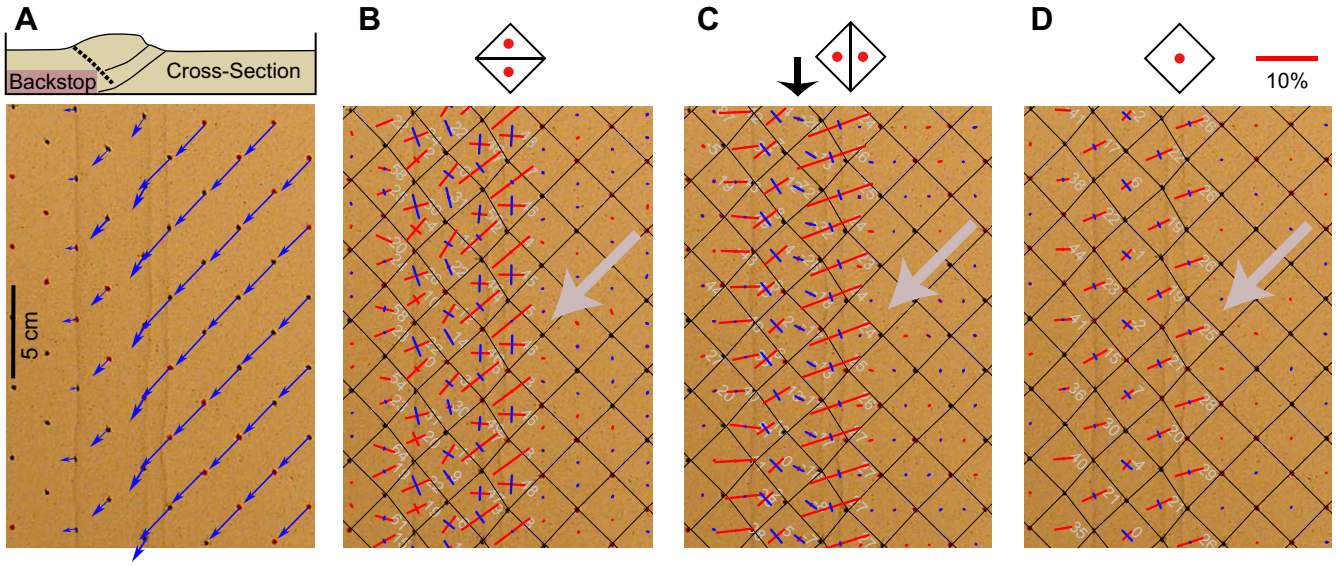

Fig. 6. A–D: Plan-view of an early stage in an analog model experiment. Frictional model of a convergent margin with a 45° obliquity to plate motion, for illustrative purposes shown at an early stage when deformation was simple. Figure A shows a schematic cross-section view of the deformation (top) near the backstop edge, and the image with the displacement vectors in blue (bottom). These displacement vectors are the measured motion of the underlying marker dots and when connected create a network from which strain is calculated. The strikes of the thrust structures run vertically in the image. Figures B to D show the principal strain axes (red = contraction and blue = extension) for each possible triangle combination (as indicated by the triangle pairs, at top) and for the entire quadrangle.

viscous (Fig. 7) orogens, is clear with 'Quad' strains comprised of the average of triangle pairs (Figs. 6D and 7D), but is obscured if strains are calculated using either set of triangles (Figs. 6A, B and 7A, B).

The same result is true of the observation that frictional convergent orogens do not undergo coeval shortening and extension (Haq and Davis, 2008) so that the extension shown in Fig. 6C is spurious. Comparison of Figs. 6D and 7D makes it possible to recognize an important difference between the strain partitioning behavior of frictional and viscous orogenic wedges. In frictional wedges, much of the along-strike component of convergence is accommodated in a relatively localized zone of shear. In a model orogen that deforms viscously, however, the accommodation of that along-strike component of motion is widely distributed and shortening axes undergo little rotation across the orogen.

Analog models can provide a sufficiently high density of velocity measurements to consider calculating strain directly from velocities, as described above. In nature, similar network densities are, at present, generally not available. Thus, techniques that interpolate the velocity field are used to obtain strain estimates in areas without direct velocity measurements (e.g., Haines and Holt, 1993; England and Molnar, 1997; Hearn and Humphreys, 1998). Such interpolations of velocity fields, which can also accommodate a variety of additional geologic and geophysical constraints such as Quaternary fault slip rates and earthquake data are used very effectively in analyzing strain in natural plate boundary zones, and can also be applied to analog modeling (Fig. 8). These velocity field-fitting techniques have advantages as well as disadvantages compared to the direct quadrangle-averaged computation of strains from displacements. For example, fitted-field calculations (even when using velocities only) are less susceptible to large local error due to single bad data points. Instead, they distribute more broadly a smaller error from the model-assumed uncertainties in the measurements. Whereas fitted-field calculations have the potential to yield spurious strains in areas with little or no data, or additional modeling constraints, direct calculations generally do not do so. Direct calculation is generally better at resolving fine features in the strain field when the station distribution has areas of

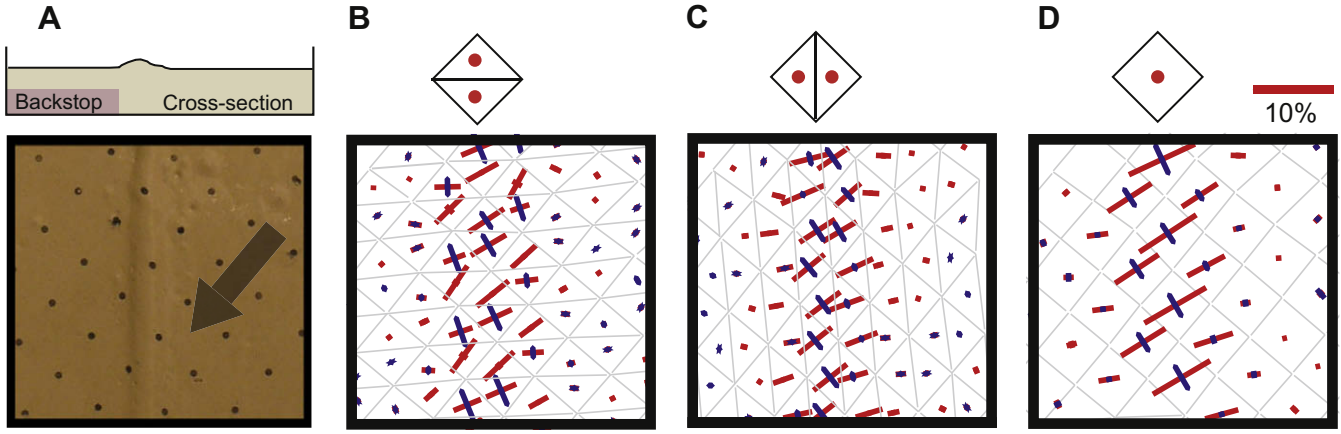

Fig. 7. Early stage of an analog experiment with a pure viscous rheology and 50° obliquity to convergence, again showing the area above the leading edge of the backstop. The wedge (8A) deforms as a continuum. Convergence is accommodated by bulk shortening and shear.

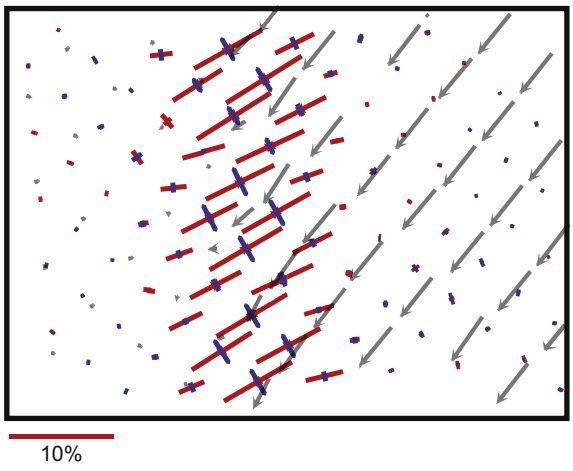

Fig. 8. Strain rate solution, for the same experiment as in Fig. 7, obtained using the technique of Haines and Holt (1993). A continuous strain rate field is obtained by fitting the observed velocities with bi-cubic spline functions. This solution is similar to the solution for quadrangles in Fig. 7d. The grey vectors are the velocities measured on the surface of the model.

very high spatial density. But neither technique fully exploits velocity data that is too densely grouped (Appendix, Fig. 1). In general, direct calculation tends to produce strain fields with transitions in tectonic style that are more discrete, whereas transitions in strain style from fitted-fields, not surprisingly, tend to be more gradual.

6. Conclusions

Compared to typical geodetic surveys of natural fold-belts, analog models can provide more data, distributed more evenly across a deforming region. Therefore, modelers may not want or need to smooth data to obtain an accurate deformation field. Modelers do, however, want to interpret correctly the active deformation style. To this end, we recommend the use of quadrangles rather than triangles to analyze data grids.

For many geoscientists, strain is an intuitive way to understand deformation that can be evident at many scales in the structures, geodetic measurements, and instantaneous deformation, such as earthquakes. In the examples shown here, strains in analog modeling experiments obtained using triangles produce results that range from faithful representations of the deformation to highly misleading, depending upon the relationship of the network gridding to the structures. This result is independent of whether the deformation is continuous or localized on discrete singularities. Using quadrangles to calculate the strain in our models allows us to yield results that are consistent with model deformation. Such careful analysis of analog models resolves key differences between models, such as the localized strain partitioning behavior of our frictional models versus the broad accommodation of oblique convergence in viscous models.

Because strain inherently assumes a continuum, significant problems can result from the mathematically correct calculation of strain from a data network that is tight with respect to the structural scale. Our examples illustrate some pitfalls of even careful use of triangles (or 3 velocities) when determining strain and strain rate, and show that the use of quadrangles, or a spline-calculated continuous field, can be significantly more reliable and is therefore preferable despite the accompanying loss of spatial resolution. By avoiding the determination of mathematically correct but geologically invalid strain from unconstrained velocity fields, the calculated strain fields determined in analog experiments become far more useful for gaining physical insight into the deformation.

Acknowledgements

We would like to thank Eric Horsman and Mark Fischer for their thorough and very helpful reviews of the manuscript, as well as Bill Holt, John Haines, and Lucy Flesch all of whom made useful suggestions. This work was partially supported by NSF grants EAR-0738920 (Purdue) and EAR-0229979 (Stony Brook).

Appendix A. Supplementary information

Supplementary data associated with this article can be found, in the online version, at doi:10.1016/j.jsg.2009.03.017.

References

Byerlee, J., 1978. Friction of rocks. Pure and Applied Geophysics 116, 615–626.
Byrne, D.E., Wang, W.H., Davis, D.M., 1993. Mechanical role of backstops in the growth of fore-arcs. Tectonics 12, 123–144.
Davis, D., Suppe, J., Dahlen, F.A., 1983. Mechanics of fold-and-thrust belts and accretionary wedges. Journal of Geophysical Research 88, 1153–1172.
England, P., Molnar, P., 1997. Active deformation of Asia: from kinematics to dynamics. Science 278, 647–650.
Enlow, R.L., Koons, P.O., 1998. Critical wedges in three dimensions: analytical expressions from Mohr-Coulomb constrained perturbation analysis. Journal of Geophysical Research 103, 4897–4914.
Haines, A.J., Holt, W.E., 1993. A procedure for obtaining the complete horizontal motions within zones of distributed deformation from the inversion of strain-rate data. Journal of Geophysical Research-Solid Earth 98, 12057–12082.
Haq, S.S.B., 2004, Mechanics of strain partitioning at convergent margins, Ph.D. dissertation, Stony Brook University.
Haq, S.S.B., Davis, D.M., 1997. Oblique convergence and the lobate mountain belts of western Pakistan. Geology 25, 23–26.
Haq, S.S.B., Davis, D.M., 2008. Extension during active collision in thin-skinned wedges: insights from laboratory experiments. Geology 36, 475–478.
Haq, S.S.B., Davis, D.M., 2005. Modeling the rheological dependence of strain partitioning in oblique wedges during active collision and "post-tectonic" relaxation. EOS (Transactions, American Geophysical Union) 86 (52) Fall Meet. Suppl., Abstract T11B-0365.
Hubbert, M.K., Rubey, W., 1959. Bulletin of the Geological Society of America 70, 115–166.
Hearn, E.H., Humphreys, E.D., 1998. Kinematics of the southern Walker Lane Belt and motion of the Sierra Nevada block, California. Journal of Geophysical Research-Solid Earth 103, 27033–27049.
Jarrard, R.D., 1986. Terrane motion by strike-slip faulting of forearc slivers. Geology 14, 780–783.
Jensen, John R., 2000. Remote Sensing of the Environment: An Earth Resource Perspective. Prentice Hall, Upper Saddle River, NJ.
Koons, P.O., Henderson, C.M., 1995. Geodetic analysis of model oblique collision and comparison to the Southern Alps of New Zealand. New Zealand Journal of Geology and Geophysics 38, 545–552.
Martinez, A., Malavieille, J., Lallemand, S., Collot, J.Y., 2002. Strain partitioning in an accretionary wedge, in oblique convergence: analogue modelling. Bulletin De La Societe Geologique De France 173 (1), 17–24.
McCaffrey, R., 1996. Estimates of modern arc-parallel strain rates in fore arcs. Geology 24, 27–30.
McClay, K.R., Whitehouse, P.S., Dooley, T., Richards, M., 2004. 3D evolution of fold and thrust belts formed by oblique convergence. Marine and Petroleum Geology 21 (7), 857–877.
Means, W.D., 1976. Stress and Strain: Basic Concepts of Continuum Mechanics for Geologists. Springer.
Mulugeta, G., 1988. Modeling the geometry of coulomb thrust wedges. Journal of Structural Geology 10 (8), 847–859.
Paterson, M.S., 1978. Experimental Rock Deformation: The Brittle field. Springer-Verlag, New York, p. 16–50.
Platt, J.P., 1993. Mechanics of oblique convergence. Journal of Geophysical Research 98 (B9), 16239–16256.
Wang, W.H., Davis, D.M., 1996. Sandbox model simulation of forearc evolution and noncritical wedges. Journal of Geophysical Research 101 (B5), 11329–11339.